THE JOURNAL OF PHYSICAL CHEMISTRY C

Article

pubs.acs.org/JPCC

K-Edge X-ray Absorption Fine Structure Analysis of Pt/Au Core−Shell Electrocatalyst: Evidence for Short Pt−Pt Distance

Takahiro Kaito,[†,‡] Hisashi Mitsumoto,[†] Seiho Sugawara,[†] Kazuhiko Shinohara,[†] Hiromitsu Uehara,[§] Hiroko Ariga,[§] Satoru Takakusagi,[§] Yoshikiyo Hatakeyama,[∥] Keiko Nishikawa,[⊥] and Kiyotaka Asakura*[,§]

[†]Nissan Motor Company, Ltd., Natsushima-cho, Yokosuka-shi, Kanagawa 237-8523, Japan

[‡]Department of Quantum Chemistry and Technology, Graduate School of Engineering, and [§]Catalysis Research Center, Hokkaido University, Kita 21 Nishi 10, Kita-ku, Sapporo, Hokkaido 001-0021, Japan

[∥]Department of Physics, College of Humanities and Sciences, Nihon University 3-25-40 Sakura Josui, Setagaya-ku, Tokyo 156-8550, Japan

[⊥]Department of Nanoscience and Technology Graduate School of Advanced Integrated Science, Chiba University, 1-33 Yayoi, Inage, Chiba 262-8522, Japan

Supporting Information

ABSTRACT: A carbon-supported Pt-shell Au-core electrocatalyst (Pt/Au/C) was prepared by sequential deposition of Pt ions on the surface of Au nanoparticles supported on carbon. The area-specific activity of the oxygen reduction reaction (ORR) for the prepared Pt/Au/C in 0.1 M $HClO_4$ aqueous solution was approximately 2 times higher than that for a commercial carbon-supported Pt electrocatalyst (Pt/C). The core−shell structure was confirmed using electrochemical methods and Pt and Au K-edge X-ray absorption fine structure (XAFS) analysis. XAFS analyses indicated that the Pt−Pt bond distance for the Pt/Au/C catalyst was shorter than that for Pt foil and the Pt/C catalyst. In addition, the Au−Au distance was much shorter than that for Au foil. The reason for the high ORR activity of Pt/Au/C is considered to be shorter Pt−Pt bond distance as compared to that of Pt/C.

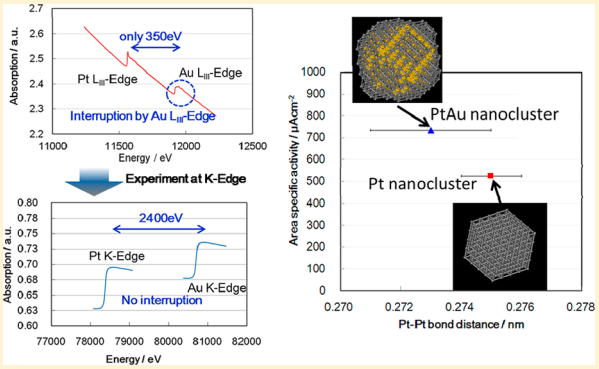

1. INTRODUCTION

Polymer electrolyte fuel cells (PEFCs) have potential as next-generation power sources for vehicles because they do not emit greenhouse gases during operation. However, there are many issues that must be resolved before PEFCs can be adopted worldwide and fuel cell electric vehicles (FCEVs) are realized. These issues include the low power density of the FC stack, low efficiency of the entire power-train system, low durability under a wide range of operating conditions and environments, and cost reduction.[1] In particular, to increase the power density and reduce costs, it is essential to improve the mass-specific activity of the Pt electrocatalyst in the FC for the oxygen reduction reaction (ORR).[2] Therefore, the structure of the Pt electrocatalyst and the reaction mechanism must be studied to understand ORR catalysis at the atomic level.[3−7] X-ray absorption fine structure (XAFS) is a powerful technique that can be used to study dynamic structural changes in an electrochemical environment. The XAFS method provides information on local structures and electronic states, such as valence states and the d vacancies of 5d transition metal atoms. In situ XAFS has been employed to investigate catalysts,[8] and such studies have revealed catalytic properties and reaction mechanisms based on dynamic structural changes[9−11] using actual fuel cell stacks[12−15] and three-electrode electrochemical cells.[16−24]

In recent years, core−shell type electrocatalysts have drawn wide attention for improvement in the mass-specific activity of Pt.[25] One effective core−shell electrocatalyst consists of a Au core and a Pt shell supported on a carbon substrate.[6,26−33] In Pt/Au core−shell electrocatalysts, both the mass-specific activity and the area-specific activity are increased with respect to the Pt nanoparticle electrocatalyst, which indicates the effectiveness of the core−shell structure to not only increase the Pt fraction on the surface of the electrocatalyst particle (geometric effect), but also to modify the Pt electronic state (electronic effect). The latter can be achieved by electron transfer and/or lattice contraction/expansion induced by interactions between the Au core and the Pt shell. However, it is difficult to directly determine the core−shell structure if the Pt shell thickness is as small as one or two monolayers. Considering the Au lattice, the Pt−Pt distance of the Pt shell in a Pt/Au core−shell electrocatalyst is expected to be longer than

Received: February 14, 2014
Revised: March 30, 2014
Published: April 1, 2014

   dx.doi.org/10.1021/jp501607f | J. Phys. Chem. C 2014, 118, 8481−8490

that in a simple Pt electrocatalyst. Surface X-ray diffraction analysis has revealed that the Pt−Pt distance in a Pt monolayer deposited on the Au(111) surface is elongated.[34] Core−shell structures and lattice mismatch can be determined directly using XAFS. Although XAFS is the most suitable technique to investigate the core−shell structures of nanoclusters and their bond distances, interference between the Pt and Au L_{III} X-ray absorption edges hinders XAFS studies on Pt and Au nanoclusters. The separation of the Pt and Au L_{III}-edges is only approximately 350 eV, which results in overlapping of EXAFS oscillation. Hence, reliable curve-fitting analysis of the Pt and Au L_{III} edges becomes difficult.[30,35,36]

If Pt and Au K-edge XAFS analyses can be performed, we can obtain well-separated Pt and Au spectra (Pt and Au K-edges are located at 78.4 and 80.7 keV, respectively), although this had been considered to be impossible due to machine limitations and finite lifetime broadening. After Ce K-edge XAFS was shown to be possible,[37] the extension of K-edge XAFS measurements to higher energies has progressed. Nishihata et al. reported Pt K-edge XAFS measurements,[38] and Nagamatsu et al. conducted ex situ K-edge XAFS measurements on fuel cell Pt/Au catalysts.[39] We have previously demonstrated that in situ Pt and Au K-edge XAFS measurements are both possible and effective for the investigation of Pt/Au core−shell electrocatalysts under operating conditions.[40]

Recently, Inaba and co-workers claimed that the simple reaction of a Pt precursor with Au nanoparticles on C without a reducing agent and under inert gas flow allows the selective deposition of Pt on the Au nanoparticles to form core−shell structures.[32,33] In this Article, Pt/Au core−shell structures on the carbon were prepared using a method similar to that reported by Inaba and co-workers,[32,33] and the resultant carbon-supported Au−Pt electrocatalyst was characterized using in situ Pt and Au K-edge XAFS spectroscopic measurements together with physical and electrochemical analyses. We discussed the structural parameters obtained by curve fitting and the origin of the enhanced area-specific activity of Pt/Au/C.

2. MATERIALS AND METHODS

2.1. Preparation of Pt/Au/C Core−Shell Electrocatalyst. The following procedure was used to prepare the Pt/Au/C electrocatalyst samples. The method for the deposition of Pt on the Au nanocluster was similar to that proposed by Inaba and co-workers.[32,33] Au nanoclusters were first prepared using the sputter-deposition-onto-ionic-liquid method,[41−43] which produces small homogeneous Au nanoclusters. A sputter coater (SC-704, Sanyu Electron; acceleration voltage = 1 kV, ion current = 20 mA) was used to sputter Au into 3 mL of ionic liquid (1-butyl-3-methylimidazolium tetrafluoroborate; C_4mimBF_4) at 328 K for 180 min. Next, 0.78 g of carbon black (XC-72R, Vulcan) was impregnated with the Au nanoparticles in C_4mimBF_4 solution for 24 h, followed by stirring in 200 mL of acetone (Wako, reagent grade) for 10 min to remove C_4mimBF_4, and the suspension was then filtered. This washing process was conducted three times to completely remove the ionic liquid. The resultant Au/C was dried in an oven at 333 K for 24 h. 0.1 g of Au/C was suspended in 200 mL of ultrapure water, and the solution was stirred with a magnetic stirrer for 15 min. The Au/C-suspended solution was then slowly added to 2 L of ultrapure water, which was deaerated by bubbling with N_2 for 30 min, and 1.0 g of 7.2 wt % H_2PtCl_6 aqueous solution was added dropwise to the solution; the resulting solution was stirred under a N_2 atmosphere for 24 h at room temperature. The resulting Pt/Au/C was filtered and dried for more than 4 h at 333 K. Finally, the Pt/Au/C product was scraped from the filter paper, yielding carbon-supported electrocatalyst powder.

Commercially available Pt/C was used as a reference (nominal Pt loading 50 wt %, Ketjen black carbon support; TEC10E50E, Tanaka Kikinzoku Kogyo K.K.).

2.2. Characterization of Pt/C and Pt/Au/C Core−Shell Electrocatalysts. The resulting catalysts were characterized using transmission electron microscopy (TEM; HF-2000 field emission TEM Hitachi High-Technologies) with energy dispersive X-ray spectroscopy (EDS; Kevex), inductively coupled plasma-mass spectrometry (ICP-MS; SPS-3520, SII NanoTechnology), and electrochemical methods. TEM was used to determine the particle diameter distribution and average diameter of the electrocatalyst particles. Microscopic elemental analysis of the Pt/Au core−shell nanoclusters was conducted using EDS. The amounts of Pt and Au electrocatalysts were measured using ICP-MS. The surface composition of Pt and Au was derived by electrochemical methods using a three-electrode glass cell and a rotating disk electrode (RDE) measurement apparatus (HZ-5000, Hokuto Denko). For the electrochemical experiments, a reversible hydrogen electrode (RHE) and Pt mesh were used as the reference and counter electrodes, respectively. Cyclic voltammograms were obtained in deaerated 0.1 M $HClO_4$ solutions. Polarization curves were recorded in an O_2-saturated $HClO_4$ solution.

2.3. XAFS Measurements. XAFS experiments were conducted at the X-ray bending magnet beamline BL16B2 of SPring-8. The ring was operated in a top-up mode at 8 GeV with the ring current at 100 mA. The X-ray beam was monochromated using a Si(511) double crystal monochromator. The incident and transmitted X-ray intensities were monitored using two ionization chambers filled with Kr before and after the sample, respectively. The setting of the samples in the in situ measurement cells has been described elsewhere.[40] Prior to the in situ measurements, air was removed by passing pure N_2 (99.99995%) through the electrolyte solution and the XAFS cell for 30 min. During the measurements, N_2 gas was continuously flowed over the electrolyte solution to prevent air contamination. The electrode potential was swept cathodically from the rest potential (ca. 1.0 V) to 0.05 V at a slow scan rate (1 mV/s) to avoid large current and potential variations in the catalyst layer and between the carbon plates. An oxidation−reduction cycle (ORC) treatment (0.05−1.2 V) was conducted three times to remove contamination from the surface of the electrocatalyst. Following the ORC treatments, XAFS measurements were performed at 0.4 V after holding the electrode potential at 0.4 V for 10 min. Pt foil, Au foil, and a AuPt random alloy foil containing 10 at. % Pt were also measured as reference samples for curve-fitting analyses.

2.4. XAFS Analyses. XAFS analyses were conducted using the REX2000 (Rigaku) analysis package. The XAFS oscillation $\chi(k)$ was extracted from the observed data $\mu(E)$ by subtracting the smoothly varying part $\mu_s(E)$, which was estimated from cubic splines.[44] The difference was then normalized using the edge height $\mu_0(E)$:[45]

$$\chi(k) = \frac{\mu(E) - \mu_s(E)}{\mu_0(E)} \quad (1)$$

dx.doi.org/10.1021/jp501607f | J. Phys. Chem. C 2014, 118, 8481−8490

where k is the wavenumber of the photoelectron, which is related to the photon energy E, and the threshold energy E_0, by

$$k = \frac{1}{\hbar}\sqrt{2m(E - E_0)} \tag{2}$$

where m is the mass of the electron. The quantity $k^3\chi(k)$ was Fourier transformed to r space, the peak in the transform was filtered, and then an inverse Fourier transform was applied to convert the filtered peak back to k space. The Fourier-filtered data were then analyzed with a curve-fitting technique using the following theoretical XAFS equations:[45]

$$k^3\chi(k) = \sum_j \frac{k_j^2 S_j N_j F_j(k_j) \exp(-2k_j^2\sigma_j^2)}{r_j^2} \sin(2k_j r_j + \varphi_j(k)) \tag{3}$$

$$k_j = (k^2 - 2m\Delta E_{0j}/\hbar^2)^{1/2} \tag{4}$$

In eqs 3 and 4, j denotes each coordination shell, N_j is the coordination number, r_j is the bond length, ΔE_{0j} is the difference between the theoretical and experimental threshold energies, and σ_j is the Debye–Waller factor for the jth coordination shell. The quantities $\phi_j(k)$ and $F_j(k)$ are phase shifts and amplitude functions, respectively, both of which were derived from FEFF8 calculations.[46] The amplitude reduction factor S_j arises from many-body effects and from inelastic losses during the scattering process. Many-body effects and inelastic losses are dependent on k in opposite ways, so that S_j can be regarded as a constant function of k.[47]

In the curve-fitting analyses, S_j and ΔE_{0j} were fixed at the values obtained for the Pt and Au foils. The quality of the fit was evaluated according to the R-factor:

$$R = \frac{\sum (k^3\chi_{obs}(k) - k^3\chi_{calc}(k))^2}{\sum (k^3\chi_{obs}(k))^2} \tag{5}$$

where $\chi_{obs}(k)$ and $\chi_{calc}(k)$ are the observed and curve-fitted $\chi(k)$ values, respectively.

In the curve-fitting analyses of bimetallic alloys, the following equations must be satisfied within the error:[48−50]

$$N_{PtAu}C_{Pt} = N_{AuPt}C_{Au} \tag{6}$$

$$R_{PtAu} = R_{AuPt} \tag{7}$$

where N_{XY} is the coordination number of atom Y around absorber atom X, C_X is the mole fraction of atom X, and R_{XY} is the interatomic distance between atoms X and Y on the X absorption edge. Errors in these structural parameters were determined at the 90% confidence level by the Hamilton ratio method.[51]

3. RESULTS

3.1. Characterization of Pt/C and Pt/Au/C Core–Shell Electrocatalysts. Figures 1–3 show TEM micrographs of Pt/C, Au/C, and Pt/Au/C, and their particle diameter distributions. The average diameter of Pt nanoclusters was estimated to be 2.2 nm from TEM image analyses of 261 Pt particles. The Au content of Au/C was 8.6 wt %, and the average diameter of the Au nanoclusters was determined to be 2.6 nm from image analyses of 339 Au particles. Nanoclusters of Au on carbon had almost the same sizes as that of Au in solution. The Pt and Au contents in the Pt/Au/C catalyst were 4.2 and 3.8 wt %, respectively, as estimated from ICP data. The

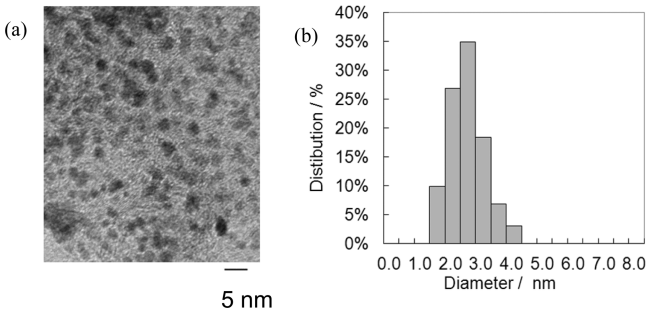

Figure 1. (a) TEM image of commercially available Pt/C electrocatalyst, and (b) particle size distribution of Pt/C estimated from (a).

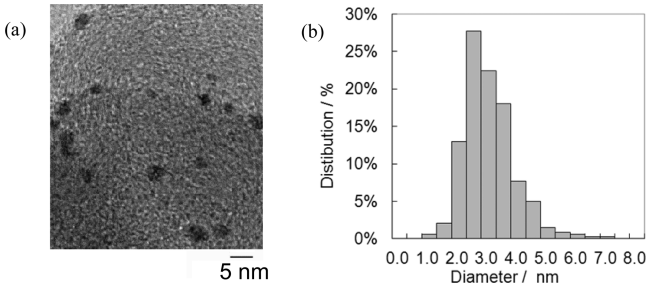

Figure 2. (a) TEM image of the Au/C prepared in this study, and (b) particle size distribution of Au/C estimated from (a).

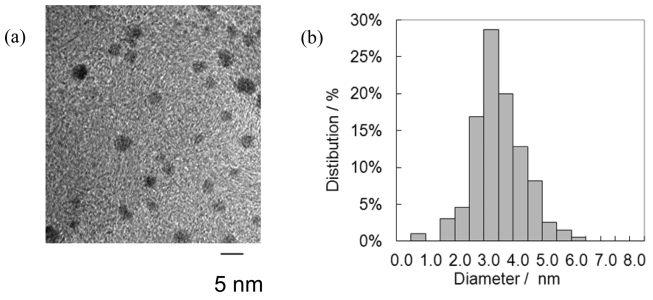

Figure 3. (a) TEM image of the Pt/Au/C prepared in this study, and (b) particle size distribution of Pt/Au/C estimated from (a).

average diameter of Pt/Au nanoclusters was estimated to be 3.0 nm from TEM image analyses of 195 nanoclusters. Comparison of the average diameter of Au/C with that of Pt/Au/C indicated that the thickness of the Pt shell would be two atomic layers.

The Pt/Au/C was dispersed in a solvent of ultrapure water and Nafion by ultrasonication for 30 min. The suspension was deposited on the precleaned glassy carbon substrate of the RDE to satisfy the 5.0 μg-Pt/cm^2 Pt loading and allowed to dry at 60 °C. Figure 4 shows cyclic voltammograms for Pt/Au/C recorded over a potential range of 0–1.6 V at a sweep rate of 50 mV/s. The potential was first swept anodically up to 1.6 V, and then the sweep direction was reversed. A small AuO reduction peak was observed at 1.2 V in the cathodic sweep. The total surface area of the Pt/Au core–shell was the sum of the Pt surface area, S_{Pt}, and the Au surface area, S_{Au}. The percentage of Pt coverage was calculated using $S_{Pt}/(S_{Pt} + S_{Au})$ and was 0.76 cm^2, as calculated from the hydrogen underpotential deposition (H_{UPD}) charge of Figure 4, divided by the hydrogen desorption and/or adsorption density on polycrystalline Pt (210 μC/cm^2).[52] S_{Au} was determined to be 0.11 cm^2 from the AuO reduction charge around 1.2 V in Figure 4,

dx.doi.org/10.1021/jp501607f | J. Phys. Chem. C 2014, 118, 8481–8490

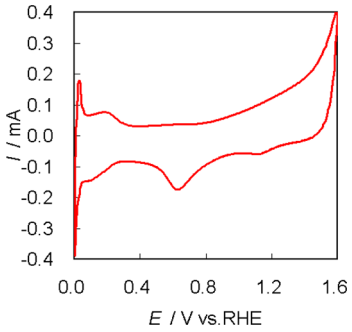

Figure 4. Cyclic voltammogram for the Pt/Au/C prepared core−shell electrocatalyst measured at a sweep rate of 50 mV/s.

divided by 386 μC/cm^2.[53] The Pt coverage percentage was approximately 88%. The electrochemical surface area (ECSA) was calculated to be 71.9 m^2/g-Pt from S_{pt} and the Pt loading on the RDE.

3.2. ORR Activity of Pt/Au/C Core−Shell Electrocatalysts. Figure 5a shows polarization curves measured with the RDE for the Pt/Au/C electrocatalyst in 0.1 M $HClO_4$ solution purged with 99.99% O_2 at various rotation speeds and at a sweep rate of 10 mV/s. The Pt loading was 5.0 μg-Pt/cm^2.

Figure 5b shows Koutecky−Levich plots, that is, the inverse current density ($1/j$) plotted as a function of the inverse square root of the rotation rate ($\omega^{1/2}$) using the data in Figure 5a. The linearity and parallelism of these plots indicate first-order kinetics with respect to molecular oxygen.[54] The specific activity of the Pt/Au/C electrocatalyst was evaluated at an electrode potential of 0.9 V and was 571 μA/cm^2, so that the mass-specific activity was 411 A/g. In contrast, the area-specific and mass-specific activities for the commercial Pt/C electrocatalyst were 298 μA/cm^2 and 251 A/g, respectively. Thus, the area-specific and mass-specific activities of the Pt/Au/C electrocatalyst were 1.9 times and 1.6 times larger than those of the Pt/C electrocatalyst, respectively.

3.3. XAFS Analysis. *3.3.1. Reference Foils.* Figure 6 shows the Pt K-edge XAFS spectrum and its oscillations for Pt foil. Although the Pt K-edge XAFS spectrum has a smooth edge jump due to lifetime broadening, XAFS oscillations could be observed after the appropriate background was removed, as shown in Figure 6b. The K-edge data were analyzed on the basis of the FEFF-derived phase shift and amplitude functions.[46] The resulting values for the Pt−Pt bond distance, coordination number, and Debye−Waller factor are shown in Table 1. Because Au and Pt have a face-centered cubic (fcc) structure, the coordination number of the first nearest neighbor atoms is 12. To obtain this coordination number, the mean free path was set to 0.24 nm, which was shorter than the mean free path of 0.65 nm in the L_{III}-edge XAFS, due to the lifetime broadening effect as reported by Nishihata et al.[38] This free path value (0.24 nm) was used for further curve fitting of the Pt K-edge data.

Figure 7a and b shows the Au K-edge XAFS spectrum and its oscillations for Au foil. A smooth edge jump was observed, as for the Pt foil in Figure 6a. The K-edge data were analyzed on the basis of the FEFF-derived phase shift and amplitude functions.[46] The resulting values for the Au−Au bond distance, coordination number, and Debye−Waller factor are shown in Table 1. The mean free path was set to 0.21 nm to give a coordination number of 12.

Comparing the Pt−Pt distances for the K-edge and L_{III}-edge shown in Table 1, the Pt−Pt distance of the L_{III}-edge was 0.003 nm shorter than that of the K-edge. The same tendency was also observed in the Au−Au bond distances. Accordingly, the bond distance obtained from curve fitting of the K-edge was considered to be longer than that derived from the L_{III}-edge, although the reason for this discrepancy remains unknown.

Figure 8a and b shows the Pt K-edge XAFS spectrum and its oscillations for Au−Pt (1/9) foil. Although the phase shifts $\phi_j(k)$ and amplitude functions $F_j(k)$ of Pt and Au atoms are so close that discrimination is difficult, the metallic radii of Pt and Au differ by about 0.005 nm; this is sufficient to create a phase difference in the oscillations, so that Pt−Pt and Pt−Au contributions can be distinguished with careful analysis. A one-shell curve fitting for the Pt−Au bond was first conducted for the Au−Pt foil in an attempt to distinguish Pt and Au by the difference in bond distance. The resulting curve-fitting parameters are shown in Table 1. The coordination number was less than 12, probably because residual Pt−Pt interactions were neglected. A two-shell curve fit was then conducted using different bond distances to separate the Pt−Pt and Pt−Au shells. In the two-shell fitting, the value of ΔE_0 for the Pt−Pt bond was fixed at the value for Pt foil. Consequently, a total coordination number of almost 12 was obtained. The Pt−Au bond distance obtained from the curve fit was between the Pt−Pt and Au−Au bond distances for the pure foils.

3.3.2. Pt/C Electrocatalyst. Figures 9 and 10 show the Pt K-edge and L_{III}-edge absorption spectra and the k^3-weighted XAFS oscillations for Pt/C, respectively. The oscillations for Pt/C were smaller than those for the Pt foil, which indicates a

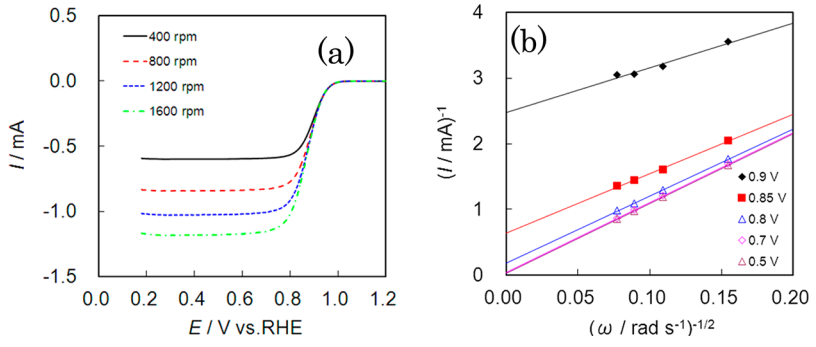

Figure 5. (a) ORR polarization curves measured using a RDE for Pt/Au/C core−shell electrocatalyst in 0.1 M $HClO_4$. Black solid line: 400 rpm. Red broken line: 800 rpm. Blue dotted line: 1200 rpm. Green chain line: 1600 rpm. (b) Koutecky−Levich plots for ORR obtained from (a). Applied voltages were following. ◆: 0.9 V. Red ■: 0.85 V. Blue △: 0.8 V. Purple ◇: 0.7 V. Brown △: 0.5 V.

dx.doi.org/10.1021/jp501607f | J. Phys. Chem. C 2014, 118, 8481−8490

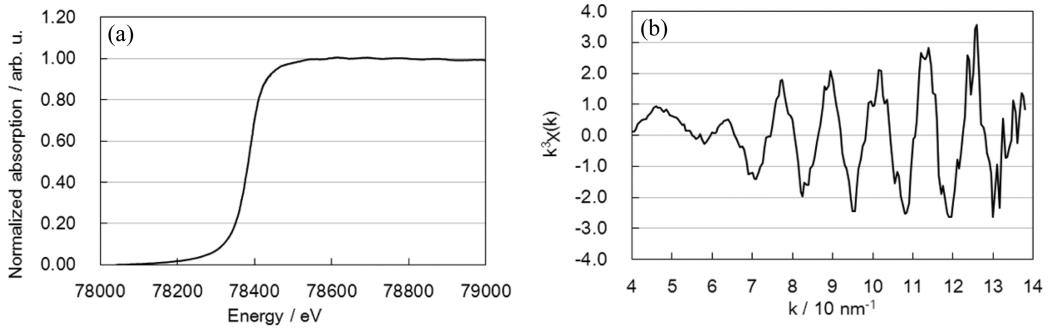

Figure 6. (a) Pt K-edge spectrum for Pt foil, and (b) k^3-weighted XAFS oscillation after background subtraction and normalization of spectrum (a).

Table 1. Curve-Fitting Results for Reference Foils

sample	edge		bond	coordination number[a]	inter atomic distance/nm	Debye–Waller factor/nm
Pt foil	Pt–L_{III}		Pt–Pt	(12)	0.275 ± 0.001	0.0071 ± 0.0004
	Pt–K		Pt–Pt	(12)	0.278 ± 0.001	0.0065 ± 0.0004
Au foil	Au–L_{III}		Au–Au	(12)	0.284 ± 0.001	0.0080 ± 0.0002
	Au–K		Au–Au	(12)	0.286 ± 0.001	0.0080 ± 0.0005
Au–Pt (1/9) foil	one shell	Pt–K	Pt–Au	10.5 ± 1.3	0.282 ± 0.001	0.0078 ± 0.0003
	two shell	Pt–K	Pt–Pt	1.2 ± 0.7	0.277 ± 0.003	0.0072 ± 0.0023
		Pt–K	Pt–Au	10.8 ± 1.1	0.283 ± 0.001	0.0077 ± 0.0003

[a]Values in parentheses were fixed.

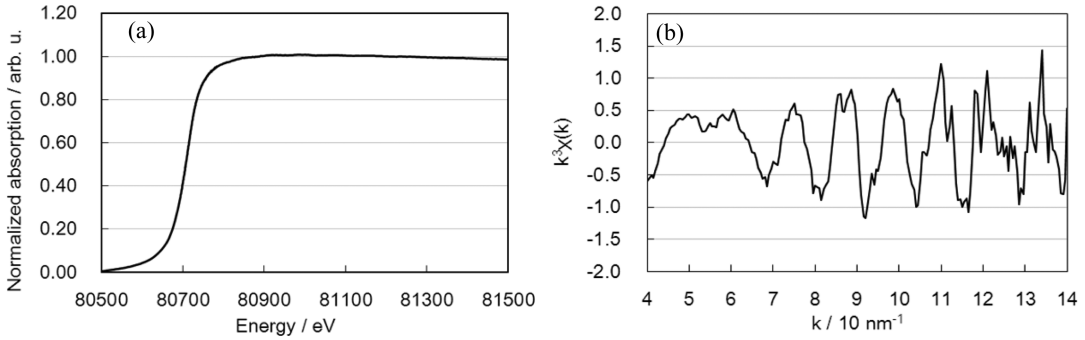

Figure 7. (a) Au K-edge spectrum for Au foil, and (b) k^3-weighted XAFS oscillation after background subtraction and normalization of spectrum (a).

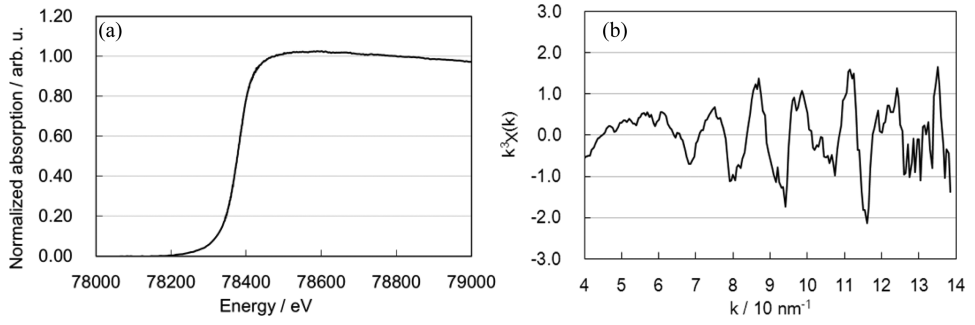

Figure 8. (a) Pt K-edge spectrum for Pt/Au (1/9) random alloy solid solution foil, and (b) k^3-weighted XAFS oscillation after background subtraction and normalization of spectrum (a).

smaller coordination number and the presence of nanoparticles. The coordination number and bond distance given in Table 2 have errors of 2.3 and 0.001 nm, respectively. However, the bond distance obtained from a K-edge curve fitting was 0.004 nm longer than that for the L_{III}-edge. The longer distance from the K-edge analysis than that from the L_3-edge corresponds to that found in the XAFS analyses of the Pt foil and Au foil.

3.3.3. Pt/Au/C Core–Shell Electrocatalyst. Figure 11a and b shows the Pt and Au K-edge k^3-weighted XAFS oscillations for Pt/Au/C. The Pt K-edge XAFS oscillations with S/N > 1 were observed up to 120 nm^{-1}, as shown in Figure 11a. As compared to Pt and Au K-edge XAFS, the oscillation of the Au K-edge was larger and lasted longer, which was more evident in the inversely Fourier filtered data in Figure S1 (Supporting Information). This means that Au had a larger coordination number and less disorder than Pt. The data were further analyzed by curve fitting to obtain structural parameters. Because the differences of phase shift and amplitude functions

dx.doi.org/10.1021/jp501607f | J. Phys. Chem. C 2014, 118, 8481–8490

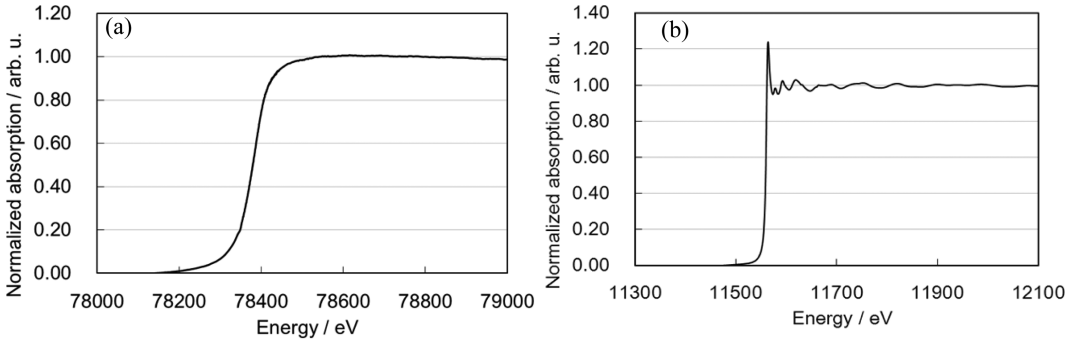

Figure 9. (a) Pt K-edge and (b) Pt L_{III}-edge XAFS spectra for Pt/C at 0.4 V vs RHE.

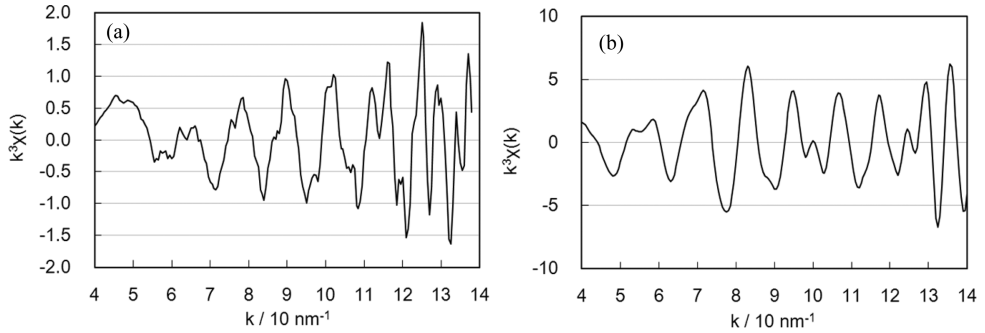

Figure 10. (a) Pt K-edge and (b) Pt L_{III}-edge k^3-weighted XAFS oscillations for Pt/C at 0.4 V vs RHE after background subtraction and normalization of the spectrum in Figure 9.

Table 2. Curve-Fitting Results for Pt/C at 0.4 V vs RHE

sample	edge	bond	coordination number	interatomic distance/nm	Debye−Waller factor/nm
Pt/C	Pt−L_{III}	Pt−Pt	9.3 ± 2.3	0.273 ± 0.001	0.0085 ± 0.0006
	Pt−K	Pt−Pt	9.6 ± 2.0	0.277 ± 0.001	0.0078 ± 0.0003

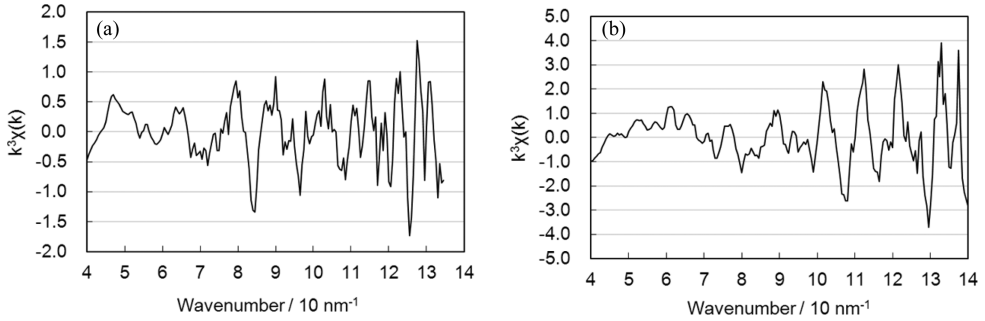

Figure 11. (a) Pt K-edge and (b) Au K-edge k^3-weighted XAFS oscillations of Pt/Au/C at 0.4 V vs RHE.

Table 3. Results from One-Shell Curve Fit for Pt/Au/C

absorbing metal	scattering metal	coordination number	bond distance/nm	Debye−Waller factor/nm
Pt	Pt	6.8 ± 1.2	0.278 ± 0.002	0.0096 ± 0.0006
Au	Au	11.3 ± 3.4	0.280 ± 0.002	0.0072 ± 0.0011

are not so much in Au and Pt, one-shell curve-fitting analyses of the Pt and Au K-edges were conducted for the Pt−Pt and Au−Au bonds, respectively, to have an approximate image. The results are given in Table 3. The Pt−Pt bond distance in the Pt/Au/C alloy was almost the same as that for Pt/C. However, the Au−Au bond distance was shorter than that for the Au foil, and the contraction in bond distance was 0.006 nm. In addition, the coordination number for Au−Au was large (almost 12), which was close to that for the Au foil and was significantly different from that for Au nanoclusters. In contrast, the coordination number for Pt−Pt was around 6. These coordination numbers are consistent with the core−shell model, in which more Pt than Au is on the surface.

To probe the structures in more detail, two-shell curve-fitting analyses for Pt and Au K-edges were conducted. To reduce the number of fitting parameters, values of ΔE_0 for Au−Au, Pt−Pt, and Pt−Au were fixed to those for the corresponding foils, and the value of ΔE_0 for Au−Pt was fixed at 5.0 eV. The uncertainty

dx.doi.org/10.1021/jp501607f | J. Phys. Chem. C 2014, 118, 8481−8490

Table 4. Results from Two-Shell Curve Fits for Pt/Au/C

	scattering metal Pt			scattering metal Au		
absorber	N	r/nm	DW/nm	N	r/nm	DW/nm
Pt	7.2 ± 2.9	0.275 ± 0.003	0.0097 ± 0.0006	2.0 ± 0.8	0.279 ± 0.004	0.008 ± 0.001
Au	2.7 ± 2.7	0.279 ± 0.005	0.005 ± 0.001	9.7 ± 2.9	0.282 ± 0.003	0.007 ± 0.001

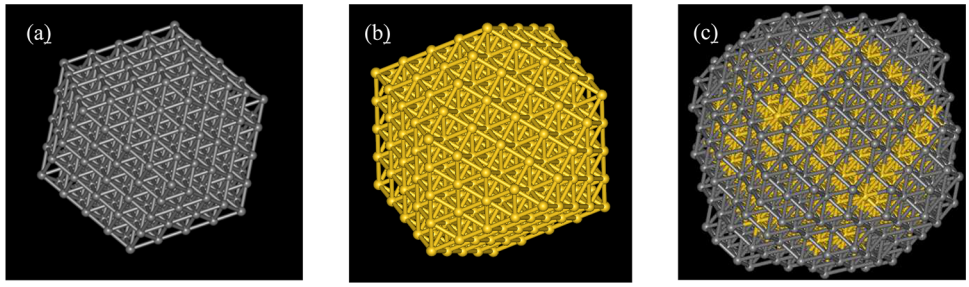

Figure 12. Estimated structures of (a) Pt cuboctahedron, (b) Au cuboctahedron, and (c) Pt/Au core−shell particle.

(±10 eV) in ΔE_0 for the Au−Pt bond gave rise to errors in bond lengths of approximately 1%. Table 4 shows the structural parameters obtained from the curve-fitting analysis. The bond distances and coordination numbers of Pt−Au and Au−Pt obtained from Pt and Au K-edge fits satisfied the conditions given in eqs 6 and 7 within the error. The distance for Pt−Au was longer than that for Pt−Pt obtained from the one-shell curve fit. The Au−Au bond distance from the two-shell curve fit was longer than that from the one-shell fit. This can be explained by the presence of Au−Pt bonding, which should have a bond length between those of Pt−Pt and Au−Au. The Au−Au distance was shorter than that for the Au foil, and the total coordination number of Au−Au + Au−Pt = 12.4 was close to that expected from the model of the Au core. However, the total coordination number of Pt−Au + Pt−Pt (=9.2) was much smaller than that for the Pt foil; these coordination numbers demonstrate the Pt shell/Au core structure. As discussed later, the "two-shell Pt on Au core" model nanocluster with a diameter of 3.0 nm provided a total coordination number of 8.7, which corresponds to the observed value.

4. DISCUSSION

4.1. Estimation of Pt/C and Pt/Au/C Core−Shell Electrocatalyst Structures. *4.1.1. Estimation of the Pt/C Nanocluster Structure.* There are two possible structures in nanoclusters, icosahedral and cuboctahedral in the literature. Judging from the particle size, we assumed the cuboctahedral structure in this Article.[55] On the basis of an average diameter of 2.2 nm and the cuboctahedron model, the particles have 4-atom edges (1.9 nm in diameter, 147 atoms) or 5-atom edges (2.4 nm in diameter, 309 atoms). Figure 12a shows a 309-atom cuboctahedron with 5-atom edges. The average coordination numbers for all Pt atoms calculated from the 4-atom edge and 5-atom edge models were 9.0 and 9.6, respectively, which are in good agreement with those obtained from the K-edge/L_{III}-edge XAFS curve fit given in Table 2 (9.6 ± 2.0 and 9.3 ± 2.3, respectively). Therefore, the Pt-on-carbon nanocluster was a cuboctahedron structure with 4-atom or 5-atom edges.

4.1.2. Estimation of the Pt/Au/C Structure. The XAFS results revealed that the coordination number derived from Au K-edge EXAFS oscillations was larger than that derived from the Pt K-edge data, which indicates a structure composed of a Au-rich core and a Pt-rich shell. Although Strbac et al. suggested that the Au(111) single crystal was partially covered with Pt,[56] the total coordination number of Au was almost 12, which indicates that the Au nanoparticle was almost fully covered with Pt. Cyclic voltammetry also showed that mostly Pt occupied the surface of the nanocluster surface. Although the reaction mechanism of H_2PtCl_6 with the Au nanoparticle is still unknown, a Pt shell can be easily prepared around the Au core by this simple reaction.

The Pt/Au core−shell structure was further analyzed on the basis of the XAFS, ICP, and TEM data. ICP analysis showed that the bulk Au:Pt ratio was 1.1. From the particle sizes of Au and Pt/Au (2.6 and 3.0 nm, respectively), we propose a cuboctahedral model with 659 atoms, as shown in Figure 12. In this structure, 309 Au atoms are located inside the nanocluster, while 350 Pt atoms cover the Au nanoclusters in two layers. The estimated core−shell model is shown in Figure 12c.

The coordination numbers of the Pt/Au structure in Figure 12c are given in Table 5. The coordination numbers obtained from the curve fits in Table 4 correspond to those observed. Thus, we propose the model structure shown in Figure 12c, where the Au core is covered with two layers of Pt atoms.

Table 5. Coordination Numbers of Estimated Pt/Au/C Structure

	coordination number	
absorbing metal	scattering metal Pt	scattering metal Au
Pt	6.7	2.1
Au	2.3	9.6

4.2. Bond Length and Electrochemical Activity of Pt/Au/C. Table 4 shows that the Au−Au and Pt−Pt distances for the Pt/Au/C core−shell electrocatalyst were shorter than the corresponding distances in the Au and Pt foils. The Pt−Pt distance in Pt/C was slightly shorter than that in the Pt foil, as shown in Table 3. The Pt−Pt distance for Pt/Au/C was even smaller than that for Pt/C. The Au−Au bond distance in the Pt/Au/C was also shorter than that in the Au foil. Pt and Au atoms generally form fcc lattices, where the Pt lattice constant is smaller than that of the Au lattice; therefore, a Pt atomic layer on a Au lattice is expected to have elongated Pt−Pt distances due to the influence of the Au lattice. This expansion of the Pt−Pt distance was observed in epitaxially grown Pt on a Au(111)

dx.doi.org/10.1021/jp501607f | J. Phys. Chem. C 2014, 118, 8481−8490

surface.[34] However, the Pt−Pt distance obtained for the two-shell curve fitting was not elongated, but instead the Au−Au distance was largely contracted. This is due to the strong Pt−Pt bond, which induces contraction of the Au core. This may be due to the labile properties of nanoclusters.

According to Adzic et al.[25] and Mukerjee et al.,[57] shorter Pt−Pt distances contribute to enhanced area-specific activity for the ORR. A comparison of the Pt−Pt distance obtained in Pt/Au/C with the relationship between the Pt−Pt distance and ORR area-specific activity reported by Mukerjee et al.[57] indicates that the Pt−Pt distance found in Pt/Au/C was in the range that can explain the high area-specific activity. The XAFS results suggest the core−shell structure and contraction of the Pt−Pt distances, which are considered to be related to the high ORR area-specific activity in the Pt/Au/C core−shell electrocatalysts. The Pt−Au nanocluster has an unexpected structure; that is, the Pt−Pt distance is shorter than that of Pt foil. The Pt L_{III} edge X-ray near edge structure was measured and showed a larger d-vacancy than those for Pt foil and Pt/C, as shown in Figure S2 (Supporting Information). This is another unexpected result because electron transfer from Au to Pt should occur. The Pt L_{III} edge for Pt−Au foil shows a smaller d vacancy by electron transfer from Au, as shown in Figure S2 (Supporting Information). We are now preparing another report to discuss the electronic structure and activity of Pt−M alloys. However, we can confirm that the Pt/Au nanoparticle should have a structure and electronic properties different from those of Pt deposited on a Au surface and PtAu bulk alloy.

5. CONCLUSIONS

A carbon-supported Pt-shell Au-core electrocatalyst (Pt/Au/C) was prepared by sequential deposition of Pt ions on the surface of Au nanoclusters. The nanoclusters were prepared by the sputter-deposition-onto-ionic-liquid method and supported on carbon. The ORR area-specific activity for the prepared Pt/Au/C in 0.1 M $HClO_4$ aqueous solution was approximately 2 times higher than that of a commercial carbon-supported Pt/C electrocatalyst. The Pt/Au core−shell structure was confirmed by electrochemical methods and XAFS analysis. The Pt−Pt bond distance for Pt/Au/C obtained from the XAFS analysis was not elongated by interactions with the Au atoms in the core. Instead, the Pt−Pt bond distance was slightly contracted, even compared to that of Pt/C. The core−shell structure and the contraction of the Pt−Pt distance on the Au core must cause high area-specific activity.

■ ASSOCIATED CONTENT

Supporting Information

Curve-fitting results of Pt and Au K-edge of Pt/Au/C and amount of d vacancy in Pt of Pt/Au/C. This material is available free of charge via the Internet at http://pubs.acs.org.

■ AUTHOR INFORMATION

Corresponding Author

*Tel.: +81-11-706-9113. E-mail: askr@cat.hokudai.ac.jp.

Notes

The authors declare no competing financial interest.

■ ACKNOWLEDGMENTS

We express thanks to Mr. K. Onishi for the preparation of the Au nanoclusters and to Nissan ARC for their help with XAFS measurements.

■ REFERENCES

(1) Srinivasan, S.; Miller, E. Applications and economics of fuel cell power plants/power sources. In *Fuel Cells*; Srinivasan, S., Ed.; Springer: New York, 2006; pp 575−605.

(2) Gasteiger, H. A.; Kocha, S. S.; Sompalli, B.; Wagner, F. T. Activity Benchmarks and Requirements for Pt, Pt-Alloy, and Non-Pt Oxygen Reduction Catalysts for PEMFCs. *Appl. Catal., B: Environ.* **2005**, *56*, 9−35.

(3) Tarasevich, M. R.; Sadkowski, A.; Yeager, E. Oxygen electrochemistry. In *Comprehensive Treatise of Electrochemistry*; Conway, B. E., Bockris, J. O., Yeager, E., Khan, S. U. M., White, R. E., Eds.; Plenum Press: New York, 1983; Vol. 7, pp 301−398.

(4) Adzic, R. R. Recent advances in the kinetics of oxygen reduction. In *Electrocatalysis*; Lipkowski, J., Ross, P. N., Eds.; Wiley-VCH: New York, 1998; p 197.

(5) Gottesfeld, S.; Zawodzinski, T. A. Polymer Electrolyte Fuel Cells. In *Advances in Electrochemical Science and Engineering*; Alkire, R. C., Kolb, D. M., Charles, W. T., Eds.; Wiley-VCH Verlag GmbH: New York, 2008; Vol. 5, pp 195−301.

(6) Brankovic, S. R.; Wang, J. X.; Adzic, R. R. New Methods of Controlled Monolayer-to-Multilayer Deposition of Pt for Designing Electrocatalysts at an Atomic Level. *J. Serb. Chem. Soc.* **2001**, *66*, 887−898.

(7) Wang, J. X.; Markovic, N. M.; Adzic, R. R. Kinetic Analysis of Oxygen Reduction on Pt(111) in Acid Solutions: Intrinsic Kinetic Parameters and Anion Adsorption Effects. *J. Phys. Chem. B* **2004**, *108*, 4127−4133.

(8) Lytle, F. W.; Via, G. H.; Sinfelt, J. H. New Application of Extended X-ray Absorption Fine Structure (EXAFS) as a Surface Probe-Nature of Oxygen Interaction with a Ruthenium Catalyst. *J. Chem. Phys.* **1977**, *67*, 3831−3832.

(9) Van't Blik, H. F. J.; Prins, R. Characterization of Supported Cobalt and Cobalt-Rhodium Catalysts: I. Temperature-Programmed Reduction (TPR) and Oxidation (TPO) of Co·$RhAl_2O_3$. *J. Catal.* **1986**, *97*, 188−199.

(10) Iwasawa, Y.; Asakura, K.; Ishii, H.; Kuroda, H. Dynamic Behaviour of Active Sites of a SiO_2-Attached Mo(VI)-Dimer Catalyst during Ethanol Oxidation Observed by Means of EXAFS. *Z. Phys. Chem.* **1985**, *144*, 105−115.

(11) Asakura, K.; Kitamura-Bando, K.; Isobe, K.; Arakawa, H.; Iwasawa, Y. Metal-Assisted CO Insertion Reaction on a New Surface Rhodium Dimer Catalyst Observed by an in Situ EXAFS Technique. *J. Am. Chem. Soc.* **1990**, *112*, 3242−3244.

(12) Allen, P. G.; Conradson, S. D.; Wilson, M. S.; Gottesfeld, S.; Raistrick, I. D.; Valerio, J.; Lovato, M. In Situ Structural Characterization of a Platinum Electrocatalyst by Dispersive X-ray Absorption Spectroscopy. *Electrochim. Acta* **1994**, *39*, 2415−2418.

(13) Allen, P. G.; Conradson, S. D.; Wilson, M. S.; Gottesfeld, S.; Raistrick, I. D.; Valerio, J.; Lovato, M. Direct Observation of Surface Oxide Formation and Reduction on Platinum Clusters by Time-Resolved X-ray Absorption Spectroscopy. *J. Electroanal. Chem.* **1995**, *384*, 99−103.

(14) Wiltshire, R. J. K.; King, C. R.; Rose, A.; Wells, P. P.; Hogarth, M. P.; Thompsett, D.; Russell, A. E. A PEM Fuel Cell for in Situ XAS Studies. *Electrochim. Acta* **2005**, *50*, 5208−5217.

(15) Ishiguro, N.; Saida, T.; Uruga, T.; Nagamatsu, S.-i.; Sekizawa, O.; Nitta, K.; Yamamoto, T.; Ohkoshi, S.-i.; Iwasawa, Y.; Yokoyama, T.; Tada, M. Operando Time-Resolved X-ray Absorption Fine Structure Study for Surface Events on a Pt_3Co/C Cathode Catalyst in a Polymer Electrolyte Fuel Cell during Voltage-Operating Processes. *ACS Catal.* **2012**, 1319−1330.

(16) Yoshitake, H.; Mochizuki, T.; Yamazaki, O.; Ota, K.-I. Study of the Density of the D-State and Structure Transformation of Pt Fine Particles Dispersed on Carbon Electrodes by in Situ X-ray Absorption Spectroscopy. *J. Electroanal. Chem.* **1993**, *361*, 229−237.

(17) Yoshitake, H.; Yamazaki, O.; Ota, K.-I. Novel Spectroelectrochemical Cell for in-Situ XAFS Spectroscopy on Gas Generating Electrodes. *J. Electroanal. Chem.* **1994**, *371*, 287−290.

(18) Mukerjee, S.; Srinivasan, S.; Soriaga, M. P.; McBreen, J. Effect of Preparation Conditions of Pt Alloys on Their Electronic, Structural, and Electrocatalytic Activities for Oxygen Reduction: XRD, XAS, and Electrochemical Studies. *J. Phys. Chem.* **1995**, *99*, 4577−4589.
(19) McBreen, J.; Mukerjee, S. In Situ X-Ray Absorption Studies of a Pt-Ru Electrocatalyst. *J. Electrochem. Soc.* **1995**, *142*, 3399−3404.
(20) Mukerjee, S.; McBreen, J. Effect of Particle Size on the Electrocatalysis by Carbon-Supported Pt Electrocatalysts: an in Situ XAS Investigation. *J. Electroanal. Chem.* **1998**, *448*, 163−171.
(21) Maniguet, S.; Mathew, R. J.; Russell, A. E. EXAFS of Carbon Monoxide Oxidation on Supported Pt Fuel Cell Electrocatalysts. *J. Phys. Chem. B* **2000**, *104*, 1998−2004.
(22) Russell, A. E.; Rose, A. X-ray Absorption Spectroscopy of Low Temperature Fuel Cell Catalysts. *Chem. Rev.* **2004**, *104*, 4613−4636.
(23) Imai, H.; Izumi, K.; Matsumoto, M.; Kubo, Y.; Kato, K.; Imai, Y. In Situ and Real-Time Monitoring of Oxide Growth in a Few Monolayers at Surfaces of Platinum Nanoparticles in Aqueous Media. *J. Am. Chem. Soc.* **2009**, *131*, 6293−6300.
(24) Sasaki, K.; Wang, J. X.; Naohara, H.; Marinkovic, N.; More, K.; Inada, H.; Adzic, R. R. Recent Advances in Platinum Monolayer Electrocatalysts for Oxygen Reduction Reaction: Scale-Up Synthesis, Structure and Activity of Pt Shells on Pd Cores. *Electrochim. Acta* **2010**, *55*, 2645−2652.
(25) Adzic, R. R.; Zhang, J.; Sasaki, K.; Vukmirovic, M. B.; Shao, M.; Wang, J. X.; Nilekar, A. U.; Mavrikakis, M.; Valerio, J. A.; Uribe, F. Platinum Monolayer Fuel Cell Electrocatalysts. *Top. Catal.* **2007**, *46*, 249−262.
(26) Kristian, N.; Wang, X. Ptshell−Aucore/C electrocatalyst with a controlled shell thickness and improved Pt utilization for fuel cell reactions. *Electrochem. Commun.* **2008**, *10*, 12−15.
(27) Shuangyin, W.; Noel, K.; Sanping, J.; Xin, W. Controlled Synthesis of Dendritic Au@Pt Core−Shell Nanomaterials for Use as an Effective Fuel Cell Electrocatalyst. *Nanotechnology* **2009**, *20*, 025605.
(28) Luo, J.; Wang, L.; Mott, D.; Njoki, P. N.; Lin, Y.; He, T.; Xu, Z.; Wanjana, B. N.; Lim, I. I. S.; Zhong, C. J. Core/Shell Nanoparticles as Electrocatalysts for Fuel Cell Reactions. *Adv. Mater.* **2008**, *20*, 4342−4347.
(29) Zheng, J.; Yang, J.; Lee, J. Y.; Zhou, W. Preparation of Carbon-Supported Core−Shell Au−Pt Nanoparticles for Methanol Oxidation Reaction: The Promotional Effect of the Au Core. *J. Phys. Chem. B* **2006**, *110*, 24606−24611.
(30) Nagamatsu, S.-i.; Arai, T.; Yamamoto, M.; Ohkura, T.; Oyanagi, H.; Ishizaka, T.; Kawanami, H.; Uruga, T.; Tada, M.; Iwasawa, Y. Potential-Dependent Restructuring and Hysteresis in the Structural and Electronic Transformations of Pt/C, Au(Core)-Pt(Shell)/C, and Pd(Core)-Pt(Shell)/C Cathode Catalysts in Polymer Electrolyte Fuel Cells Characterized by in Situ X-ray Absorption Fine Structure. *J. Phys. Chem. C* **2013**, *117*, 13094−13107.
(31) Xiu, C.; Shengnan, W.; Scott, J.; Zhibing, C.; Zhenghua, W.; Lun, W.; Yongxin, L. The Deposition of Au−Pt Core−Shell Nanoparticles on Reduced Graphene Oxide and their Catalytic Activity. *Nanotechnology* **2013**, *24*, 295402.
(32) Inaba, M.; Tsuji, H. Platinum Core-Shell Catalyst Manufacturing Method, and Fuel Cell using Catalyst. Japan Patent WO2011115012 A1, March 19, 2010.
(33) Tsuji, H.; Kaneko, A.; Banno, M.; Yamada, H.; Saito, M.; Tasaka, A.; Inaba, M. A Novel Technique for Preparation of Pt shell/Au core/C Core-Shell Catalysts and Their Activity for Oxygen Reduction Reaction. *218th ECS Meeting Abstracts*; Las Vegas, 2010; MA2010-02, p 858.
(34) Shibata, M.; Hayashi, N.; Sakurai, T.; Kurokawa, A.; Fukumitsu, H.; Masuda, T.; Uosaki, K.; Kondo, T. Electrochemical Layer-by-Layer Deposition of Pseudomorphic Pt Layers on Au(111) Electrode Surface Confirmed by Electrochemical and In Situ Resonance Surface X-ray Scattering Measurements. *J. Phys. Chem. C* **2012**, *116*, 26464−26474.
(35) Zhang, J.; Sasaki, K.; Sutter, E.; Adzic, R. R. Stabilization of Platinum Oxygen-Reduction Electrocatalysts Using Gold Clusters. *Science* **2007**, *315*, 220−222.
(36) Nagamatsu, S.-i.; Arai, T.; Yamamoto, M.; Ohkura, T.; Oyanagi, H.; Ishizaka, T.; Kawanami, H.; Uruga, T.; Tada, M.; Iwasawa, Y. Potential-Dependent Restructuring and Hysteresis in the Structural and Electronic Transformations of Pt/C, Au(Core)-Pt(Shell)/C, and Pd(Core)-Pt(Shell)/C Cathode Catalysts in Polymer Electrolyte Fuel Cells Characterized by in Situ X-ray Absorption Fine Structure. *J. Phys. Chem. C* **2013**, *117*, 13094−13107.
(37) Asakura, K.; Satow, Y.; Kuroda, H. Ce K-edge EXAFS Spectrum of CeO_2. *J. Phys. (Paris)* **1986**, *47*, 185−188.
(38) Nishihata, Y.; Emura, S.; Maeda, H.; Kubozono, Y.; Harada, M.; Uruga, T.; Tanida, H.; Yoneda, Y.; Mizuki, J.; Emoto, T. XAFS Spectra in the High-Energy Region Measured at SPring-8. *J. Synchrotron Radiat.* **1999**, *6*, 149−151.
(39) Nagamatsu, S.-I.; Arai, T.; Yamamoto, M.; Oyanagi, H.; Daimaru, A.; Ishizaka, T.; Kawanami, H.; Uruga, T.; Tada, M.; Iwasawa, Y. In Situ XAFS Study on PEFC Catalysts: Structure and Behavior of Pt-M/C (M=Au, Pd) in the Stepwise Voltage Operation. *220th ECS Meeting Abstracts*, Boston, 2011; MA2011-02, p 1055.
(40) Kaito, T.; Mitsumoto, H.; Sugawara, S.; Shinohara, K.; Uehara, H.; Ariga, H.; Takakusagi, S.; Asakura, K. A New Spectroelectrochemical Cell for in Situ Measurement of Pt and Au K-edge X-ray Absorption Fine Structure. *Rev. Sci. Instrum.*, submitted.
(41) Torimoto, T.; Okazaki, K.-I.; Kiyama, T.; Hirahara, K.; Tanaka, N.; Kuwabata, S. Sputter Deposition onto Ionic Liquids: Simple and Clean Synthesis of Highly Dispersed Ultrafine Metal Nanoparticles. *Appl. Phys. Lett.* **2006**, *89*, 243117−3.
(42) Hatakeyama, Y.; Takahashi, S.; Nishikawa, K. Can Temperature Control the Size of Au Nanoparticles Prepared in Ionic Liquids by the Sputter Deposition Technique? *J. Phys. Chem. C* **2010**, *114*, 11098−11102.
(43) Hatakeyama, Y.; Onishi, K.; Nishikawa, K. Effects of Sputtering Conditions on Formation of Gold Nanoparticles in Sputter Deposition Technique. *RSC Adv.* **2011**, *1*, 1815−1821.
(44) Cook, J. J. W.; Sayers, D. E. Criteria for Automatic X-ray Absorption Fine Structure Background Removal. *J. Appl. Phys.* **1981**, *52*, 5024−5031.
(45) Asakura, K. Analysis of XAFS. In *X-ray Absorption Fine Structure for Catalysts and Surfaces*; Iwasawa, Y., Ed.; World Scientific: Singapore, 1996; pp 35−58.
(46) Rehr, J. J.; Albers, R. C. Theoretical Approaches to X-ray Absorption Fine Structure. *Rev. Mod. Phys.* **2000**, *72*, 621−654.
(47) Teo, B. K.; Antonio, M. R.; Averill, B. A. Molybdenum K-edge Extended X-ray Absorption Fine Structure Studies of Synthetic Molybdenum-Iron-Sulfur Clusters Containing the MoS4 Unit: Development of a Fine Adjustment Technique Based on Models. *J. Am. Chem. Soc.* **1983**, *105*, 3751−3762.
(48) Toshima, N.; Harada, M.; Yonezawa, T.; Kushihashi, K.; Asakura, K. Structural Analysis of Polymer-Protected Palladium/Platinum Bimetallic Clusters as Dispersed Catalysts by Using Extended X-ray Absorption Fine Structure Spectroscopy. *J. Phys. Chem.* **1991**, *95*, 7448−7453.
(49) Toshima, N.; Harada, M.; Yamazaki, Y.; Asakura, K. Catalytic Activity and Structural Analysis of Polymer-Protected Gold-Palladium Bimetallic Clusters Prepared by the Simultaneous Reduction of Hydrogen Tetrachloroaurate and Palladium Dichloride. *J. Phys. Chem.* **1992**, *96*, 9927−9933.
(50) Via, G. H.; Drake, K. F.; Meitzner, G.; Lytle, F. W.; Sinfelt, J. H. Analysis of EXAFS Data on Bimetallic Clusters. *Catal. Lett.* **1990**, *5*, 25−33.
(51) Hamilton, W. Significance Tests on the Crystallographic R Factor. *Acta Crystallogr.* **1965**, *18*, 502−510.
(52) Li, W.; Lane, A. M. Resolving the HUPD and HOPD by DEMS to Determine the ECSA of Pt Electrodes in PEM Fuel Cells. *Electrochem. Commun.* **2011**, *13*, 913−916.
(53) Tremiliosi-Filho, G.; Dall'Antonia, L. H.; Jerkiewicz, G. Growth of Surface Oxides on Gold Electrodes under Well-Defined Potential, Time and Temperature Conditions. *J. Electroanal. Chem.* **2005**, *578*, 1−8.

(54) Anastasijević, N. A.; Vesović, V.; Adžić, R. R. Determination of the Kinetic Parameters of the Oxygen Reduction Reaction Using the Rotating Ring-Disk Electrode: Part I. Theory. *J. Electroanal. Chem. Interfacial Electrochem.* **1987**, *229*, 305−316.
(55) Baletto, F.; Ferrando, R. Structural Properties of Nanoclusters: Energetic, Thermodynamic, and Kinetic Effects. *Rev. Mod. Phys.* **2005**, *77*, 371−423.
(56) Strbac, S.; Petrovic, S.; Vasilic, R.; Kovac, J.; Zalar, A.; Rakocevic, Z. Carbon monoxide oxidation on Au(111) surface decorated by spontaneously deposited Pt. *Electrochim. Acta* **2007**, *53*, 998−1005.
(57) Mukerjee, S.; Srinivasan, S.; Soriaga, M. P.; McBreen, J. Role of Structural and Electronic Properties of Pt and Pt Alloys on Electrocatalysis of Oxygen Reduction. *J. Electrochem. Soc.* **1995**, *142*, 1409−1422.